

Chaos and localization in the wavefunctions of complex atoms NdI, PmI and SmI

Dilip Angom and V. K. B. Kota

Physical Research Laboratory, Navarangpura, Ahmedabad - 380 009

Wavefunctions of complex lanthanide atoms NdI, PmI and SmI, obtained via multi-configuration Dirac-Fock method, are analyzed for density of states in terms of partial densities, strength functions ($F_k(E)$), number of principal components ($\xi_2(E)$) and occupancies ($\langle n_\alpha \rangle^E$) of single particle orbits using embedded Gaussian orthogonal ensemble of one plus two-body random matrix ensembles [EGOE(1+2)]. It is seen that density of states are in general multi-modal, $F_k(E)$'s exhibit variations as function of the basis states energy and $\xi_2(E)$'s show structures arising from localized states. The sources of these departures from EGOE(1+2) are investigated by examining the partial densities, correlations between $F_k(E)$, $\xi_2(E)$ and $\langle n_\alpha \rangle^E$ and also by studying the structure of the Hamiltonian matrices. These studies point out the operation of EGOE(1+2) but at the same time suggest that weak admixing between well separated configurations should be incorporated into EGOE(1+2) for more quantitative description of chaos and localization in NdI, PmI and SmI.

PACS numbers: 05.30.-d, 05.45.Mt, 32.10.-f, 32.30.-r

I. INTRODUCTION

Lanthanide atoms exhibit complicated configuration mixing and have complex spectra [1] as consequence of partially filled high angular momentum $4f$ and $5d$ valence shells. The general form of the ground state configuration is $[\text{Xe}]6s^2 4f^m 5d^n$, where m and n are the shell occupancies. Across the period m increases from 1 to 14, whereas n is 1 for Ce I and Gd I which are located at the beginning and middle of the period and n is 0 for the remaining lanthanide atoms. Along the period the number of configurations and mixing increases as $4f$ shell occupancy increases, and reaches a maximum around the middle. Lanthanide atoms are appropriate to study complexities emerging from two-body interactions and a comparative study along the period could provide insights to the implications of increasing particle number to the nature of the complexity.

Detailed studies of Ce I wave-function structure, first carried out by Flambaum and collaborators [2, 3] showed the smoothed (with energy) strength functions ($F_k(E)$) and number of principle components (NPC or $\xi_2(E)$), which measure chaoticity, can be understood in terms of banded random matrices (BRM) with the local level and strength fluctuations following the predictions of Wigner's Gaussian orthogonal ensemble (GOE) of random matrices. Later studies of Cummings and collaborators on Pr I (and also Ce I) [4], the element next to Ce I in the lanthanide series, showed results in agreement with Flambaum et al studies of CeI. Flambaum and collaborators further developed, using the BW form for $F_k(E)$ and NPC in terms of the BW spreading widths which are a result of many body chaos, a statistical theory for the distribution of occupation numbers [5, 6], and also for electromagnetic transition strengths in atoms with complex (or chaotic) spectra [7]. Applying this statistical spectroscopy for complex states, energy-averaged cross sections are obtained in terms of sums over single electron orbitals and using this Flambaum et al [8] and Gribakin et al [9] explained the observed, and quite puzzling, low-energy electron recombination rate of Au^{25+} .

Following the successful applications in nuclei [10–13], mesoscopic physics [14], in the context of quantum computers [15] and as suggested more recently for example in the dynamics of cold atoms [16], a better random matrix hypothesis for atoms is to consider the interaction (after subtracting the single particle field generated by the Coulomb Hamiltonian see Eq. (5) ahead for the Hamiltonian) to be random. This gives rise to embedded GOE of one plus two-body interactions [EGOE(1+2)]. See Sect. III ahead for details of EGOE(1+2) and here it suffices to say that the ensemble is $\{H\} = h(1) + \lambda\{V(2)\}$ where $h(1)$ is the mean-field one-body part and $\{V(2)\}$ is a GOE in 2-particle space with λ the interaction strength. An extreme limit, with strong interaction ($\lambda \rightarrow \infty$), of EGOE(1+2) is two body random matrix ensemble (TBRE). Recently we demonstrated that Sm I [17], which has three more active electrons compared to Pr I, carries TBRE signatures which include Gaussian state densities, strength functions having Gaussian form, NPC as a function of energy is of Gaussian form, local level fluctuations follow GOE etc. Going beyond this limiting situation, EGOE(1+2) with increasing interaction strength (equivalently with increasing particle number if the interaction is fixed), strength functions exhibit Breit-Wigner to Gaussian transition. It is important to stress that EGOE(1+2) at the weak limit (λ small) shares features with BRM, for example the BW form for strength functions (this explains partly the applicability of BRM for CeI and PrI). In a recent paper [18], an interpolating function, analogous to the Brody distribution for nearest neighbor spacing distribution, representing the BW to Gaussian transition of the strength function is reported (see Eq. (23) ahead) and it is used to understand this transition in rare earth atoms (at the spectrum's center) as we go from CeI to SmI with valence electrons changing from 4 to 8. In addition,

it is noticed in NdI, PmI and SmI studies that the eigenfunctions exhibit localization properties. The presence of localized states is also evident in the study of Ce I and Pr I by Cummings and collaborators [4].

As shown in [19], the number of allowed $4f^m6s^2 - 4f^m6s6p$ and $4f^m - 4f^{m-1}5d$ dipole transitions of the rare earth atoms is large (for example, in Pr I the number of allowed $4f^36s^2 - 4f^36s6p$ dipole transitions is 7402) and it is difficult to study the transitions individually. However, statistical spectroscopy, based on TBRE and many-body chaos, provides a means to understand the smoothed part of these transitions (with fluctuations following GOE). In this paper we consider NdI, PmI and SmI with 6,7 and 8 valence electrons and examine in some detail: (i) the extent to which EGOE(1+2) applies for these atoms; (ii) localization properties of wavefunctions; (iii) the structure of the Hamiltonian matrix. For (i) and (ii), wavefunctions are analyzed in terms of density of states as sum of partial densities, strength functions, NPC and occupancies of single particle orbits and correlations between them. These results form Section IV of the paper. Section V discusses the structure of the Hamiltonian matrices and the modifications to be incorporated in EGOE(1+2) for a more quantitative description of chaos and localization in lanthanide atoms. For completeness, Section II gives the method of atomic structure calculations and Section III gives the definition and a brief discussion of some of the basic results for EGOE(1+2). Finally Section V gives conclusions and future outlook.

II. METHOD OF ATOMIC CALCULATIONS

A. Multi-Configuration Dirac-Fock method

The earlier works on lanthanide atoms [20] have shown that the multiconfiguration Dirac-Fock (MCDF) method is suitable for studying the structure and calculating properties of these atoms. The method is the relativistic equivalent of multiconfiguration Hartree-Fock (MCHF) [21] used extensively in non-relativistic atomic calculations. For a detailed description of MCDF see ref [22] and several groups have implemented it to study atom and molecules [23]. For completeness and continuity important features of the method are described in this section. The essence of MCDF is the calculation of orbitals in a mean field arising from a linear combination of configurations. Then, the single particle states are the eigenstates of variationally calculated single-electron Schrödinger equations and these are represented as $|n\kappa\rangle$, where n is the principal quantum number. The quantum number $\kappa = \mp(l \pm s) + 1/2$ is similar to the total angular momentum quantum number $j = l \pm s$, however unlike j it is unique for each orbital symmetry. The single electron wavefunction is the two-component Dirac spinor

$$\psi_{n\kappa}(\mathbf{r}) = \langle \mathbf{r} | n\kappa \rangle = \frac{1}{r} \begin{pmatrix} P_{n\kappa}(r) \chi_{\kappa m}(\theta, \phi) \\ iQ_{n\kappa}(r) \chi_{-\kappa m}(\theta, \phi) \end{pmatrix} \quad (1)$$

where $P_{n\kappa}(r)$ and $Q_{n\kappa}(r)$ are large and small component radial functions respectively, and $\chi_{\kappa m}(\theta, \phi)$ and $\chi_{-\kappa m}(\theta, \phi)$ are the spinor spherical harmonics in the lsj coupling scheme. The many electron basis functions of the method are the configuration state functions (CSF's) [21]. Each CSF is represented as $|\gamma PJM\rangle$, where P , J and M are the parity, total angular momentum and magnetic quantum numbers, and γ is a quantum number to identify each CSF uniquely. The CSFs are constructed in two steps: first couple the identical electrons in each sub-shell $n_i\kappa_i$ to give X_i , and second couple X_i to obtain J . The construction of the CSFs are better described in second quantized notations, let a_{njm}^\dagger and a_{njm} be creation and annihilation operators of the single electron states. Then, the a_{njm}^\dagger operators form a complete set of spherical tensor of rank j . However, for the annihilation operators

$$\tilde{a}_{jm} = (-1)^{j-m} a_{j,-m} \quad (2)$$

forms a complete set and not a_{njm} . The operators satisfy the modified anticommutation relation

$$[\tilde{a}_{nj} \times a_{n'j'}^\dagger]^{JM} + (-1)^{j+j'-J} [a_{n'j'}^\dagger \times \tilde{a}_{nj}]^{JM} = \sqrt{2j+1} \delta_{jj'} \delta_{J0} \delta_{M0} \delta_{nn'}, \quad (3)$$

where $[\tilde{a}_{nj} \times a_{n'j'}^\dagger]^{JM}$ represents tensor coupling of the operators to rank J and component M . In absence of external magnetic field, like in the present calculations, the CSFs are degenerate in M and each CSF can be identified without M as $|\gamma PJ\rangle$. A CSF $|\gamma PJ\rangle$ having p sub-shells is created from the vacuum state

$$|\gamma PJ\rangle = [(a_p^\dagger)^{q_p}, \nu_p X_p [(a_{p-1}^\dagger)^{q_{p-1}}, \nu_{p-1} X_{p-1} [\dots [(a_1^\dagger)^{q_1}, \nu_1, X_1]^{J_1}] \dots]^{J_{p-1}}]^{J} |0\rangle \quad (4)$$

where q_i is the number of electrons in the i^{th} sub-shell and ν_i is the seniority quantum number, which identify identical sub-shell total angular momentum X_i uniquely. It is also possible to use an ordering index instead of ν for details; see ref [24].

An appropriate relativistic Hamiltonian to describe high Z atoms like lanthanides is Dirac-Coulomb Hamiltonian H^{DC} , which includes only the electrostatic interactions. For N electron atom

$$H^{\text{DC}} = \sum_{i=1}^N c\boldsymbol{\alpha}_i \cdot \mathbf{p}_i + c^2(\beta_i - 1) - \frac{Z(\mathbf{r}_i)}{r_i} + \sum_{i=1}^N \sum_{j=i+1}^N \frac{1}{|\mathbf{r}_i - \mathbf{r}_j|} \quad (5)$$

where $\boldsymbol{\alpha}_i$ and β_i are Dirac matrices, \mathbf{p}_i is the electron momentum, $Z(\mathbf{r}_i)$ is the nuclear-charge at \mathbf{r} and N is the number of electrons. The first two terms are single electron Dirac Hamiltonian, the third and last terms are electron-nucleus and electron-electron Coulomb interactions respectively. The H^{DC} is diagonal in the total angular momentum J states $|\Gamma P J\rangle$, the atomic state functions (ASF). Here, Γ is a quantum number to identify each ASF uniquely and parity P is a good quantum number as H^{DC} is invariant under parity transformation. The ASFs are linear combination of CSFs $|\gamma_r P J\rangle$

$$|\Gamma P J\rangle = \sum_{\gamma} c_{r\Gamma} |\gamma_r P J\rangle, \quad (6)$$

The ASFs satisfy the Schrödinger equation

$$H^{\text{DC}}|\Gamma P J\rangle = E_{\Gamma}|\Gamma P J\rangle \quad (7)$$

where E_{Γ} is the eigenvalue.

The starting point of the MCDF method is the variational optimization of an energy functional defined in terms of H^{DC} and Lagrange multipliers with respect to one or more ASFs. The parameters of variational optimization are the coefficients $c_{\gamma r}$ and orbitals $\psi_{n\kappa}(\mathbf{r})$. In general, the energy functional is extremized with respect to the ground state. Another class of MCDF calculations is the extended optimal level (EOL), where the energy functional is extremized using a set of ASFs. We use the later method in our calculations and the advantages over the general method is explained in the next subsection. The energy functional of MCDF-EOL calculation is

$$W^{\text{DC}} = \sum_{r,s} d_{rs} H_{rs}^{\text{DC}} + \sum_{a=1}^{n_w} \sum_{r=1}^{n_c} d_{rr} q(a) \epsilon_a + \sum_{a=1}^{n_w-1} \sum_{b=a+1}^{n_w} \delta_{ab} \epsilon_{ab} N(ab), \quad (8)$$

where d_{rs} and d_{rr} are the weight factors, H_{rs}^{DC} are the matrix element of H^{DC} between the CSFs $|\gamma_r P J\rangle$ and $|\gamma_s P J\rangle$ and n_w is the number of the orbitals. The quantity $N(ab)$ is the overlap integral between the a^{th} and b^{th} orbitals and ϵ_a and ϵ_{ab} are the Lagrange multipliers to enforce orthonormality between orbitals of the same symmetry but different principal quantum numbers. The weight factors can be chosen in several ways, in EOL calculation

$$d_{rs} = \frac{1}{n_L} \sum_i^{n_L} c_{\Gamma_i}^r c_{\Gamma_i}^s \quad (9)$$

where n_L is number of ASFs. Thus, atomic structure and property calculations are carried out using a hierarchy of eigenstates: orbitals, configuration state functions and atomic state functions.

B. Orbital calculation and configuration interaction

The calculation of an appropriate set of orbitals $\{\psi(\mathbf{r})\}$ is crucial in atomic structure and properties calculations. In the present work we calculate the orbitals using the MCDF method described in the previous subsection. This method can include strong configuration mixing, however the orbitals generated are state specific, this is undesirable for statistical studies involving several excited states. To strike a balance between these two features of MCDF method, orbitals are generated within selected CSF space and the energy functional is optimized with respect to several states using MCDF-EOL method. The orbitals generated are less state specific as these are calculated in the potential of several states self-consistently. The orbital set of each atom are generated in a series of calculations described in this section.

The calculations are relativistic, however for compact notation we define configurations in non-relativistic notations. The Xe like core is considered as reference state $|\Phi_0\rangle$ and in non-relativistic notations

$$|\Phi_0\rangle = [(a_{5p}^\dagger)^6 [(a_{5s}^\dagger)^2 [\dots [(a_{1s}^\dagger)^2] \dots]] |0\rangle. \quad (10)$$

TABLE I: The number of relativistic CSFs N_{CSF} arising from each of the non-relativistic configurations. The range of the diagonal elements or ϵ_k^{\min} and ϵ_k^{\max} are also given, the ϵ_k values are defined relative to the lowest ϵ_k in the CSF space. In the table, the configurations are defined relative to the ground configuration $4f^m 6s^2$, where m is 4, 5 and 6 for Nd, Pm and Sm respectively.

Config	Nd		Pm		Sm	
	N_{CSF}	$\epsilon_k^{\min} - \epsilon_k^{\max}$	N_{CSF}	$\epsilon_k^{\min} - \epsilon_k^{\max}$	N_{CSF}	$\epsilon_k^{\min} - \epsilon_k^{\max}$
$4f^m 6s^2$	19	0.0 -0.25	29	0.0 -0.28	46	0.0 -0.38
$4f^m 6s5d$	288	0.31-0.64	521	0.09-0.53	748	0.03-0.58
$4f^{m-1} 6s^2 6p$	40	0.39-0.69	92	0.33-0.65	172	0.39-0.85
$4f^m 5d^2$	608	0.63-1.08	1090	0.24-0.69	1579	0.18-0.86
$4f^{m-1} 6s5d6p$	684	0.67-1.04	1619	0.43-0.87	3014	0.44-1.00
$4f^m 6p^2$	236	0.97-1.30	409	0.83-1.25	602	0.87-1.38
$4f^{m+1} 6p$	172	1.11-1.50	241	1.02-1.40	276	1.09-1.61
$4f^{m-2} 6s^2 6p^2$	31	1.14-1.30	91	1.09-1.42	234	1.19-1.58
$4f^{m-2} 6s^2 5d^2$	78	1.38-1.64	240	1.01-1.34	608	1.03-1.56
$4f^{m+2}$	46	1.56-1.90	46	1.61-1.97	46	1.74-2.10

where $|0\rangle$ is the vacuum state. The intermediate angular momenta J_i are zero as all the sub-shells are completely filled. The orbitals of the ground state configuration $[\text{Xe}]6s^2 4f^m 5d^n$ are then generated treating $6s$, $4f$ and $5d$ orbitals as active valence shells. The calculation is in the CSF manifold of all single and double replacements among the active valence sub-shells of the ground configuration. The CSFs considered have the form

$$|\gamma_i P_i J_i\rangle = [(a_{5d}^\dagger)^{p_i}, \nu_{5d} X_{5d} [(a_{6s}^\dagger)^{q_i}, \nu_{6s} X_{6s} [(a_{4f}^\dagger)^{r_i}, \nu_{4f} X_{4f}]^{J_{1i}}]^{J_{2i}}]^{J_i} |\Phi_0\rangle, \quad (11)$$

where p_i , q_i and r_i are the sub-shell occupancies and satisfy the condition $p_i + q_i + r_i = 2 + m + n$. Further, the conditions $m \geq r_i \geq m - 2$, $2 \geq q_i \geq 0$ and $n \geq p_i \geq n - 2$ are imposed to select single and double replacement CSFs within the ground configuration. Then, a MCDF-EOL calculation of the the lowest multiplet levels is carried out. Valence orbital $6p$ is generated in another calculation with frozen core approximation, where the orbitals of the ground configuration generated in the previous calculation are held fixed. The CSF space of the calculation consists of single excitation from the ground configuration to $6p$. The orbital $5d$ is generated in a similar calculation if it is unoccupied ($n = 0$) in the ground configuration. Thus, in relativistic notations, the orbital set consists of $(1-6)s_{1/2}$, $(2-6)p_{1/2,3/2}$, $(3-5)d_{3/2,5/2}$ and $4f_{5/2,7/2}$. Out of these $6s_{1/2}$, $4f_{5/2,7/2}$, $6p_{1/2,3/2}$ and $5d_{3/2,5/2}$ are valence shells, then the number of valence shells N_v and core shells N_c are 7 and 17 respectively. All the orbitals are made spectroscopic, that is, each orbital has $n - l - 1$ (where n and l are the principal and orbital angular momentum quantum numbers) number of nodes. The other possibility is calculating the orbitals without imposing the constraint on the number of nodes. Orbitals of this type are referred to as correlation orbitals. These are usually contracted, state specific and represent correlation effects of specific states very well. For statistical properties calculations, the spectroscopic orbitals are appropriate. The MCDF calculations to generate the orbitals include important intra valence correlation effects but it is incomplete within the orbital basis considered. A configuration interaction (CI) calculation, which is diagonalization of H^{DC} matrix, of all the possible CSFs can capture the remaining correlation effects. However, such a calculation is impossible as the size of the CSF space increases exponentially with the number of active valence electrons and N_v . In our calculations the CSF space consists of single and double excitations from the ground configuration

$$|\gamma_i P_i J_i\rangle = [(a_{6p}^\dagger)^{p_i}, \nu_{6p} X_{6p} [(a_{5d}^\dagger)^{q_i}, \nu_{5d} X_{5d} [(a_{6s}^\dagger)^{r_i}, \nu_{6s} X_{6s} [(a_{4f}^\dagger)^{s_i}, \nu_{4f} X_{4f}]^{J_{1i}}]^{J_{2i}}]^{J_{3i}}]^{J_i} |\Phi_0\rangle, \quad (12)$$

where $p_i + q_i + r_i + s_i = 2 + m + n$, and impose the conditions $m \geq s_i \geq m - 2$, $2 \geq r_i \geq 0$, $n \geq q_i \geq n - 2$ and $2 \geq p_i$. Thus, all the CSFs considered are connected to the ground configuration $[\text{Xe}]6s^2 4f^m 5d^n$. The CSF space has ten non-relativistic configurations, among these $4f^m 5d^2$ and $4f^{m-1} 6s5d6p$ together contribute more than half of the CSFs. The maximum number of CSFs arises from $4f^{m-1} 6s5d6p$, which has the largest number of open shells. The number of CSFs arising from each non-relativistic configuration and range of $\langle \gamma P J | H^{\text{DC}} | \gamma P J \rangle$ are given in Table I.

Consider N_a and N_α as the number of active valence electrons and single particle states respectively. Then, N_a is 6, 7 and 8 for Nd, Pm and Sm respectively and $N_\alpha = 32$ since the valence space consists of $6s_{1/2}$, $6p_{1/2,3/2}$, $5d_{3/2,5/2}$ and $4f_{5/2,7/2}$ (each orbital contribute $2j + 1$ number of single particle states). In addition, define the number of unfilled single particle states as $N_o = N_\alpha - N_a$. Then, the number of possible determinantal states is $\binom{N_\alpha}{N_a}$ and the

two-electron Coulomb interaction couples each Slater determinant to

$$K = 1 + N_a N_o + N_a(N_a - 1)(N_o)(N_o - 1)/4 \quad (13)$$

determinants which include itself and others with shell occupancies different by one and two. In a single determinant approximation of the ground state, K is also the number of determinants in the manifold which includes the single and double excitations. This is the determinantal equivalent of the CSF manifold chosen in our calculations. For further analysis, consider these K determinants as the manifold chosen for calculations. As mentioned in the context of CSFs, the representation of two-electron Coulomb interaction is incomplete in such a determinantal manifold. This is because, the Coulomb interaction couples pairs of determinants which differ by one or two occupancies. Hence, for the singly excited determinants, the zeroth order description of Coulomb interaction is incomplete without the triply excited ones. The quadruply excited are similarly needed for the doubly excited determinants. Among the K determinants, the fraction coupled to a singly excited one is

$$K_s = \frac{K - (N_a - 1)(N_a - 2)(N_o - 1)(N_o - 2)/4}{K} \quad (14)$$

$$\sim \frac{1}{N_a} \quad \text{when } N_o \gg N_a.$$

The last term in the numerator is the number of triply excited states coupled to a singly excited determinant but absent in the manifold. Similarly, the fraction of the determinants coupled to double excited determinant is

$$K_d = \frac{K - [(N_a - 2)(N_o - 2) + (N_a - 2)(N_a - 3)(N_o - 2)(N_o - 3)/4]}{K} \quad (15)$$

$$\sim \frac{1}{N_a} \quad \text{when } N_o \gg N_a.$$

That is, each of the states considered are directly coupled to $\sim 1/N_a$ of the total number. However, higher order two-electron Coulomb interaction connects all the determinants within the same J manifold. For $N_a \sim 3$, the K_s and K_d scaling show the number of determinants mixed at first order is close to the GOE predicted value of number of principal components (NPC). Similar scalings apply to the CSFs as these are linear combinations of Slater determinants. This implies that a CSF space consisting of single and double excitations alone can provide a good representation of the eigenvalues and eigenfunction properties.

III. EIGENFUNCTION PROPERTIES IN EGOE(1+2)

This section gives a brief introduction to EGOE(1+2) and a summary, for later use, of the results known for this random matrix ensemble; see [11] for a review on this subject and also [18].

A. Definition of EGOE(1+2)

Let us start with two-body embedded GOE, i.e. EGOE(2) or TBRE defined for spinless fermion systems. The EGOE(2) for m ($m > 2$) fermion with the particles distributed say in N single particle states $|\nu_i\rangle$, $i = 1, 2, \dots, N$ is generated by defining the Hamiltonian H , which is 2-body, to be GOE in the 2-particle space and then propagating it to the m -particle spaces by using the geometry (direct product structure) of the m -particle spaces. Operator form for a 2-body Hamiltonian $H=V(2)$ is defined by,

$$V(2) = \sum_{\nu_i < \nu_j, \nu_k < \nu_l} \langle \nu_k \nu_l | V(2) | \nu_i \nu_j \rangle_a a_{\nu_l}^\dagger a_{\nu_k}^\dagger a_{\nu_i} a_{\nu_j} ; \quad (16)$$

$$\langle \nu_k \nu_l | V(2) | \nu_j \nu_i \rangle_a = - \langle \nu_k \nu_l | V(2) | \nu_i \nu_j \rangle_a ,$$

$$\langle \nu_k \nu_l | V(2) | \nu_i \nu_j \rangle_a = \langle \nu_i \nu_j | V(2) | \nu_k \nu_l \rangle_a$$

Now, the Hamiltonian H matrix in m -particle spaces, in the occupation number basis (occupation numbers will be 0 or 1 and the basis is generated by distributing the m particles in all possible ways in the single particle states $|\nu_r\rangle$), is defined in terms of the two-body matrix elements $\langle \nu_k \nu_l | V(2) | \nu_i \nu_j \rangle_a$ (note that the subscript 'a' stands for

antisymmetrized two-particle states) and the non-zero matrix elements are of three types,

$$\begin{aligned}
\langle \nu_1 \nu_2 \cdots \nu_m | V(2) | \nu_1 \nu_2 \cdots \nu_m \rangle_a &= \sum_{\nu_i < \nu_j \leq \nu_m} \langle \nu_i \nu_j | V(2) | \nu_i \nu_j \rangle_a \\
\langle \nu_p \nu_2 \nu_3 \cdots \nu_m | V(2) | \nu_1 \nu_2 \cdots \nu_m \rangle_a &= \sum_{\nu_i = \nu_2}^{\nu_m} \langle \nu_p \nu_i | V(2) | \nu_1 \nu_i \rangle_a \\
\langle \nu_p \nu_q \nu_3 \cdots \nu_m | V(2) | \nu_1 \nu_2 \nu_3 \cdots \nu_m \rangle_a &= \langle \nu_p \nu_q | V(2) | \nu_1 \nu_2 \rangle_a ; \\
\text{all other } \langle \cdots | H | \cdots \rangle_a &= 0 \text{ due to the two-body selection rules.}
\end{aligned} \tag{17}$$

The EGOE(2) is defined by the above Eqs. and a GOE representation for $V(2)$,

$$\begin{aligned}
\langle \nu_k \nu_l | V(2) | \nu_i \nu_j \rangle_a &\text{ are independent Gaussian random variables} \\
\overline{\langle \nu_k \nu_l | V(2) | \nu_i \nu_j \rangle_a} &= 0 , \\
\overline{|\langle \nu_k \nu_l | V(2) | \nu_i \nu_j \rangle_a|^2} &= v^2(1 + \delta_{(ij),(kl)})
\end{aligned} \tag{18}$$

where the bar denotes ensemble average and v^2 is a constant. Note that $d(m) = \binom{N}{m}$ is the Hamiltonian matrix dimension and the number of independent two-body matrix elements is $[d(2)(d(2) + 1)]/2$.

Hamiltonian for realistic systems such as atoms consists of a mean-field one-body (defined by a finite set of single particle states) plus a complexity generating two-body interaction. Then the appropriate random matrix ensemble, for many purposes, is EGOE(1+2) defined by

$$\{H\} = h(1) + \lambda\{V(2)\} \tag{19}$$

where $\{ \}$ denotes an ensemble. In (19), the mean-field one-body Hamiltonian $h(1) = \sum_i \epsilon_i n_i$ is a fixed one-body operator defined by the single particle energies ϵ_i with average spacing Δ (note that n_i is the number operator for the single particle state $|i\rangle$). In general one can choose ϵ_i to form an ensemble; see [14] for examples. The $\{V(2)\}$ in (19) is EGOE(2) with $v^2 = 1$ in Eq. (18) and λ is the strength of the two-body interaction (in units of Δ). Thus, EGOE(1+2) is defined by the four parameters (m, N, Δ, λ) and without loss of generality we choose $\Delta = 1$. Construction of EGOE(1+2) follows from Eqs. (16), (17) and (18) by just adding to the diagonal matrix elements (see the first equality in (17)) the term $\sum_i \epsilon_i$ where ν_i are the occupied single particle states for the given basis state.

B. Basic properties of EGOE(1+2)

Most significant aspect of EGOE(1+2) is that as λ changes, in terms of state density, level fluctuations, strength functions and entropy, the ensemble admits three chaos markers as described in Fig. 1 and reviewed in [18]. Firstly, it is well known, via the EGOE(2) results in [10, 25] and the fact that general $h(1)$'s produce Gaussian densities, that the state densities $\rho^{H,m}(E) = \langle \delta(H - E) \rangle^m$ take Gaussian form, for large enough m , for all λ values (often the superscripts (H, m) are dropped),

$$\rho^{H,m}(E) = \frac{1}{\sqrt{2\pi} \sigma_H(m)} \exp -\frac{\hat{E}^2}{2}, \tag{20a}$$

$$\hat{E} = (E - \epsilon_H(m))/\sigma_H(m) \tag{20b}$$

In (20), $\epsilon_H(m) = \langle H \rangle^m$ is the spectrum centroid and similarly $\sigma_H(m)$ is the spectrum width. In practice there will be deviations from the Gaussian form and they are taken into account by using Edgeworth expansion [26] in terms of the skewness (γ_1) and excess (γ_2) parameters. With $\rho^H(E)dE = \eta(\hat{E})d\hat{E}$, the $\eta_G(\hat{E})$ with lower order Edgeworth corrections is,

$$\eta_{ED}(\hat{E}) = \eta_G(\hat{E}) \left\{ 1 + \frac{\gamma_1}{6} He_3(\hat{E}) + \frac{\gamma_2}{24} He_4(\hat{E}) + \frac{\gamma_1^2}{72} He_6(\hat{E}) \right\} \tag{21}$$

where $He_r(\widehat{E})$ are Hermite polynomials. With λ increasing, there is a chaos marker λ_c such that for $\lambda \geq \lambda_c$ the level fluctuations follow GOE, i.e. λ_c marks the transition in the nearest neighbor spacing distribution from Poisson to Wigner form. Parametric dependence of λ_c is $\lambda_c \propto 1/m^2 N$ [27]. Now let us define strength functions.

To maintain consistency with the notations used in EGOE(1+2) literature, from hereafter, we represent CSFs as $|k\rangle$ and ASFs as $|E\rangle$. Then, Eq. 6 assumes the form $|E\rangle = \sum_k c_k^E |k\rangle$. Given the mean-field $h(1)$ basis states $|k\rangle = \sum_E C_k^E |E\rangle$, the strength functions (one for each k) $F_k(E) = \sum_{\beta \in E} |C_k^{E,\beta}|^2 = \overline{|C_k^E|^2} (d\rho^H(E))$. As λ increases further from λ_c , the strength functions change from Breit-Wigner (BW) to Gaussian form and the transition point is denoted by λ_F ; see Fig. 1. The BW and Gaussian (denoted by \mathcal{G}) forms of $F_k(E)$ are,

$$F_{k:BW}(E) = \frac{1}{2\pi} \frac{\Gamma_k}{(E - E_k)^2 + \Gamma_k^2/4}, \quad (22a)$$

$$F_{k:\mathcal{G}}(E) = \frac{1}{\sqrt{2\pi} \sigma_k} \exp - \frac{(E - E_k)^2}{2\sigma_k^2} \quad (22b)$$

where $E_k = \langle k | H | k \rangle$. With $p = \int_{-\infty}^{\mathcal{E}_p} F_k(E) dE$, the spreading width $\Gamma_k = \mathcal{E}_{3/4} - \mathcal{E}_{1/4}$. Similarly the variance of F_k is $\sigma_k^2 = \langle k | H^2 | k \rangle - (\langle k | H | k \rangle)^2$. For $\lambda_c \leq \lambda \leq \lambda_F$ (this is called BW domain) they are close to BW form and for $\lambda > \lambda_F$ (this is called Gaussian domain) they approach Gaussian form. In fact the BW form starts in a region below λ_c (as shown in Fig. 1, there is a λ_0 such that below λ_0 , the strength functions are close to δ -function form and for $\lambda > \lambda_0$ there is onset of BW form) but the fluctuations are close to Poisson for $\lambda < \lambda_c$. Arguments based on BW spreading widths give $\lambda_F \propto 1/\sqrt{m}$ [5, 28] and this result will be used later. Unlike the Poisson to GOE transition in level fluctuations, which is common for Hamiltonians with regular and irregular (chaos generating) parts, the BW to Gaussian transition in strength functions is a unique signature for the operation of EGOE(1+2) in finite quantum systems. For the BW to Gaussian transition, a good interpolating function has been constructed recently [18],

$$F_{k:BW-\mathcal{G}}(E : \alpha, \beta) dE = \frac{(\alpha\beta)^{\alpha-\frac{1}{2}} \Gamma(\alpha)}{\sqrt{\pi} \Gamma(\alpha - \frac{1}{2})} \frac{dE}{((E - E_k)^2 + \alpha\beta)^\alpha}, \quad \alpha \geq 1 \quad (23)$$

In $F_{k:BW-\mathcal{G}}(E : \alpha, \beta)$, β supplies the scale while α defines the shape (hence α is the significant parameter) as it gives BW for $\alpha = 1$ and Gaussian for $\alpha \rightarrow \infty$. The variance of $F_{k:BW-\mathcal{G}}$ is $\sigma^2(F_{k:BW-\mathcal{G}}) = \sigma_k^2 = \alpha\beta/(2\alpha-3)$, $\alpha > 3/2$. It is important to stress that in general (α, β) change with k although for EGOE(1+2) they are nearly constant except for F_k with E_k very far from their centroid. Fig. 2 shows that the interpolating function (23) fits very well the numerical EGOE(1+2) results for strength functions; for more detailed discussion see [18].

One important measure of the complexity of eigenstates of interacting systems is the participation ratio PR (denoted by ξ_2), $\xi_2(E) = \{\sum_k |C_k^E|^4\}^{-1}$ where the subscript ‘2’ for ξ denotes that it is the second R enyi entropy [29]; in literature PR is also often called number of principal components (NPC) as it gives the number of basis states that make up the eigenstate with energy E . Following Ref. [30] one can write ξ_2 in terms of the strength functions,

$$\{\xi_2(E)/\xi_2^{GOE}\}^{-1} = \frac{1}{[\rho^H(E)]^2} \int_{-\infty}^{\infty} dE_k \rho^h(E_k) [F_k(E)]^2, \quad \xi_2^{GOE} = d/3 \quad (24)$$

In writing (24), it is assumed that the level and strength fluctuations are of GOE type and hence it is valid only for $\lambda > \lambda_c$. Further, $\rho^h(E_k)$ is the density of E_k energies and it is generated by an effective one-body Hamiltonian \mathbf{h} [30]. Also, in general $\rho^h(E_k)$ is also a Gaussian for EGOE(1+2). Assuming that α and β are k -independent, $\xi_2(E)$ in the BW to Gaussian transition domain can be evaluated by substituting $F_{k:BW-\mathcal{G}}$ for $F_k(E)$ in (24). At the spectrum center the integral in (24) can be evaluated and it gives [18],

$$\xi_2(E=0)/\xi_2^{GOE} = \left\{ \sqrt{\frac{2}{2\alpha-3}} \frac{\Gamma^2(\alpha)}{\Gamma^2(\alpha-\frac{1}{2})} \frac{1}{\sqrt{\zeta^2(1-\zeta^2)}} \times U\left(\frac{1}{2}, \frac{3}{2} - 2\alpha, \frac{(2\alpha-3)(1-\zeta^2)}{2\zeta^2}\right) \right\}^{-1} \quad (25)$$

where $U(- - -)$ is hypergeometric-U function [31]. In (25), the correlation coefficient $\zeta = \sqrt{1 - \overline{\sigma_k^2}/\sigma_H^2}$ where $\overline{\sigma_k^2} = (1/d) \sum_{i \neq j} H_{ij}^2$ and $\sigma_H^2 = (1/d) \sum_i (E_i - \epsilon)^2$ are the variance of the off-diagonal Hamiltonian matrix elements

and eigenvalues respectively. However, in the Gaussian domain, with $F_k(E)$ being a Gaussian, gives for any E ,

$$\xi_2(E)/\xi_2^{GOE} = \sqrt{1 - \zeta^4} \exp - \frac{\zeta^2 \hat{E}^2}{1 + \zeta^2} \quad (26)$$

Instead of NPC, it is possible to use the closely related information entropy $S^{info}(E)$; $S^{info}(E) = -\sum_E |C_k^E|^2 \log |C_k^E|^2$. An interesting recent observation is that [32] as we increase λ much beyond λ_F , there is a chaos marker λ_t around which different definitions of entropy (for example S^{info} , thermodynamic entropy defined via $\rho^H(E)$, single particle entropy defined via occupation numbers), temperature etc. will coincide and also strength functions in $h(1)$ and $V(2)$ basis will coincide. Thus $\lambda \sim \lambda_t$ region is called the thermodynamic region and [13] gives first application of this marker.

It is important to point out that the eigenstates of atoms carry good angular momentum (J) (in some situations even good L, S) and therefore in principle one should consider EGOE(1+2) preserving J -symmetry (called EGOE(1+2)- J in [11]). Theory for EGOE(1+2)- J is not available (see however [33, 34] for some first attempts), and just as in the nuclear shell model studies [11, 35], it is assumed that the forms for $\rho^H(E)$, $F_k(E)$, $(NPC)_E$ etc. derived using EGOE(1+2) for spinless fermion systems, extend to J spaces. This can be considered to be an aspect of chaos in atoms and this is the basis for statistical atomic spectroscopy as being developed by Flambaum; see [3, 8, 36] and references therein.

IV. RESULTS FOR $\rho^H(E)$, $F_k(E)$, $\xi_2(E)$ AND $\langle n_\alpha \rangle^E$

In the present study, we select the $J = 4^+$ CSF manifold for Nd and Sm atoms. The parity is chosen equal to the parities of the ground configurations $4f^4 6s^2$ and $4f^6 6s^2$ respectively and the total angular momentum J is the same as in the Ce I work [2]. For Pm, which has an odd number (i.e. 7) of active valence electrons we choose $J = 9/2^-$ CSFs. The parity is again equal to the ground configuration parity $4f^5 6s^2$. It is to be reiterated that, the orbitals of the present study are different from our earlier work [17]. As mentioned in Section IIB, the orbitals in this work are calculated in a multiconfiguration potential, whereas in [17], the orbitals are calculated in a single configuration potential. The manifolds of the Nd, Pm and Sm have 2200, 4375 and 7325 CSFs respectively. The CSFs are generated in the sequence of sub-shell occupations but later, these are energy ordered. The CI calculation is carried out within the whole space for Nd and Pm. For Sm, as mentioned in [17], the density of states $\rho(E)$ is bimodal. We select the first 6300 CSFs which contribute to the first peak for the CI calculation. The atomic state $|E\rangle$ of the Nd, Pm, and Sm obtained from the CI calculations have energy range of 2.20, 2.27 and 1.60 hartree respectively.

A. Density of states $\rho^H(E)$

By definition, density of state $\rho(E) = \langle \delta(H - E) \rangle$ is a sequence of δ -functions. For obtaining the smoothed (with respect to energy E) density of states and for comparison with the EGOE(1+2) predictions of $\rho^{H,m}(E)$, we construct the binned density of states. In the our calculations, the energy range of $|E\rangle$ of each atom is divided into sixty bins of equal sizes. The density of states is then binned and normalized, these are shown in Fig.3. The Gaussian and Edgeworth corrected Gaussian calculated from the centroid ϵ , variance σ^2 , skewness γ_1 and excess γ_2 of $\rho(E)$ are also shown in the figure (ϵ , σ^2 , γ_1 and γ_2 values are given in the figure). For SmI Gaussian is in good agreement with the $\rho(E)$ except at and around the centroid. At the centroid the Gaussian is $\sim 13\%$ less than the actual $\rho(E)$. In general all $\rho(E)$ are multimodal in structure and it is most prominent in Nd. The $\rho(E)$ for Nd has a pronounced peak at $\hat{E} \sim -1.5$ and fluctuations above the mean for \hat{E} between 1.0 and 2.5. Similarly for Pm, $\rho(E)$ has a pronounced peak at $\hat{E} \sim 1.4$. As discussed ahead, the multimodal structures correlate with similar structures of the number of principal components and observed deviations of the strength function from the ϵ_k dependent variation. Finally for SmI, there is a peak at $\hat{E} \sim 2$.

The multimodal form of $\rho^{H,m}(E)$ can be understood by decomposing it into a sum of partial densities. For each sub-shell occupancy \tilde{m} one can define a partial density $\rho^{H,\tilde{m}}(E)$ with centroids $E_c(\tilde{m})$ and $\sigma^2(\tilde{m})$ defined by,

$$E_c(\tilde{m}) = \langle H \rangle^{\tilde{m}} \quad , \quad \sigma^2(\tilde{m}) = \langle (H - E_c(\tilde{m}))^2 \rangle^{\tilde{m}} \quad . \quad (27)$$

Note that $\sigma^2(\tilde{m})$ is sum of partial variances $\sigma^2(\tilde{m} \rightarrow \tilde{m}')$ where

$$\begin{aligned}\sigma^2(\tilde{m}) &= \sum_{\tilde{m}'} \sigma^2(\tilde{m} \rightarrow \tilde{m}'), \\ \sigma^2(\tilde{m} \rightarrow \tilde{m}') &= \{d(\tilde{m})\}^{-1} \sum_{\alpha, \beta} |\langle \tilde{m} \alpha | H | \tilde{m}' \beta \rangle|^2 \quad \text{for } \tilde{m} \neq \tilde{m}' \\ \sigma^2(\tilde{m} \rightarrow \tilde{m}) &= \left\{ d(\tilde{m})^{-1} \sum_{\alpha, \beta} |\langle \tilde{m} \alpha | H | \tilde{m} \beta \rangle|^2 \right\} - \{E_c(\tilde{m})\}^2\end{aligned}\tag{28}$$

Usually the $\sigma^2(\tilde{m} \rightarrow \tilde{m})$ is called internal variance and others, partial variances [37]. In terms of the partial densities the total density of states is,

$$\rho^{H,m}(E) = [d(m)]^{-1} \sum_{\tilde{m}} \rho^{H,\tilde{m}}(E) d(\tilde{m})\tag{29}$$

where m is the number of active valence electrons, \tilde{m} represent the possible sub-shell occupancies, $d(m)$ and $d(\tilde{m})$ are the number of CSFs in the CI calculation and number of CSFs in the \tilde{m} sub-shell occupancy manifold respectively. That is, $\rho^{H,m}(E)$ is the sum of partial densities $\rho^{H,\tilde{m}}(E)$ from the sub-shell occupations defined in Eq. (12). It is important to stress that Eq. (29) is exact. As evident from Eq. (12), each of the possible sub-shell occupations have different angular momentum coupling sequence. It is easily seen that $\rho^{H,m}(E)$ takes multimodal shape when the partial densities are well separated with weak mixing between them (i.e. partial variance is much smaller than the internal variance). The range of ϵ_k (i.e. diagonal elements of the Hamiltonian matrix H_{rr}^{DC}) of each non-relativistic configuration given in Table I, which is a representation of the partial density spread, is plotted for Nd in Fig.4a. At ~ 0.62 hartree, it shows small overlap between the $4f^46s5d$ and next in energy $4f^45d^2$ and $4f^36s5d6p$ configurations. The separation is also visible in the Hamiltonian structure discussed ahead [Fig. 9 ahead shows two distinct blocks centered around ~ 0.5 hartree and ~ 0.8 hartree respectively]. In addition, the Coulomb mixing $\langle 4f^46s5d | 1/r_{12} | 4f^45d^2 \rangle$ and $\langle 4f^46s5d | 1/r_{12} | 4f^36s5d6p \rangle$ are weak as the configurations differ by a single occupancy. The separation between the configurations persists in $|E\rangle$ and the contributions from $4f^46s5d$ configuration manifests as the smaller peak of the bimodal $\rho^{H,m}(E)$. The energy range of the remaining configurations show large overlaps and contribute to the main peak of the Nd $\rho^{H,m}(E)$. The $4f^36s^26p$ configuration which lie between $4f^46s5d$ and $4f^45d^2$ energetically, is single replacement from $4f^45d^2$ and doesn't contribute to smoothing the $\rho^{H,m}(E)$. Fig.4b shows the result of Eq. (29) with partial densities represented by Gaussians for Nd. The agreement between theory and calculations is excellent. This demonstrates that it is possible to construct the total density of states as sums of Gaussian partial densities (even though a single Gaussian representation as shown in Fig. 3 deviates strongly from the calculated results). This result is significant as it is possible to calculate the centroids and variances (also partial variances) without recourse to H matrix construction [37]. Similar to the Nd, the bimodal structure of the Pm's $\rho^{H,m}(E)$ is a consequence of the small overlap between the partial densities of the $4f^46s5d6p$ and $4f^56p^2$ configurations. However, unlike Nd, these configurations are in the higher end of the energy range. In contrast to Nd and Pm, the Sm atom has partial densities with large overlap and the $\rho^{H,m}(E)$ is without prominent secondary peaks. Now we will turn to strength functions which are nothing but the partial densities with \tilde{m} 's divided into individual basis states.

B. Strength functions $F_k(E)$

The $F_k(E)$ of the individual CSFs $|k\rangle$ exhibit large fluctuations and significant variation is observed between $F_k(E)$ of neighboring $|k\rangle$. This is evident from the selected $|k\rangle$ presented in our Sm I work [17]. For statistical description we consider the representative strength function $\overline{F_k(E)}$ which is the average of individual $F_k(E)$ within the range of energy $\epsilon_k \pm \Delta\epsilon$. In the present work, we have chosen $\hat{\epsilon}_k \pm .25\sigma_k$ as the range of averaging to calculate $\overline{F_k(E)}$ and the centroids of the individual $F_k(E)$ are aligned while averaging. Fig. 5 shows $\overline{F_k(E)}$ of Nd I, Pm I and SmI calculated at $\hat{\epsilon}_k = -1.5, -1.0, -0.5$, and 0. For all the three atoms, the interpolating function of Eq. (23) fits the $\overline{F_k(E)}$ very well; the β parameter in Eq. (23) has been eliminated using the calculated σ_k . The best fit value of α for Nd I, Pm I and SmI for $\hat{\epsilon}_k = 0$ are 5, 7.5 and 11 respectively, thus these are in the Breit-Wigner to Gaussian transition region with SmI closest to Gaussian. This result is already reported in [18] (it should be noted that in this paper $\overline{F_k(E)}$ is constructed by averaging $F_k(E)$ over 3% of the basis states around $\hat{\epsilon}_k = 0$ and this is different from the procedure used in Fig. 5 and therefore there is slight difference in the α values extracted). Moving away from $\hat{\epsilon}_k = 0$, firstly it

is seen that the parameter α in Eq. (23) is k dependent and it changes from a value close to that of BW to a value giving close to Gaussian form as $\hat{\epsilon}_k$ is increasing from -1.5. For Nd, Pm and Sm α changes from 2 to 5.2, 2.5 to 7.5 and 2.5 to 10.6 respectively. The variation in α seen in Fig. 5 is understood from the fact that near the Fermi surface (i.e. for $\hat{\epsilon}_k \sim -1.5$ to -1) the levels are well separated and hence the mixing is weak giving BW form and as we go towards the center the mixing is strong giving close to Gaussian (or between BW and Gaussian) form. It should be pointed out that EGOE(1+2) ensemble do not produce large changes in α as k changes in $F_k(E)$. However, in all the calculations it is seen that σ_k is essentially constant as expected from EGOE(1+2). Clearly, the $F_k(E)$ analysis shows that modifications of EGOE(1+2) are needed.

C. Number of principal components $\xi_2(E)$ and localized states

The inverse participation ratio $\xi_2(E)$ of an eigenstate is the effective number of basis functions contributing to it. It provides a measure for the presence of chaos in the system. For a GOE with dimension d , the NPC is $d/3$ independent of energy while for EGOE(1+2) there is strong energy dependence (it is Gaussian in the Gaussian domain; see Eq. (26)). The $\xi_2(E)$ of Nd, Pm and Sm for all $|E\rangle$ are calculated and shown in Fig. 6a-c. The $\xi_2(E)$ of Nd and Pm are multimodal and localized states (i.e. states with NPC much smaller than GOE or EGOE(1+2) predicted values) are prominent in all the atoms. We should add that localized states are also observed in the previous studies on Ce I [2] and Pr I [4]. In addition, more recently, localization quite similar to those shown Fig.6 are also seen in U^{28+} calculations [38]. Despite localization, Nd and Pm have Breit-Wigner like envelopes, whereas for Sm it is like Gaussian. Nd and Pm have Gaussian like secondary peaks around ~ -1.5 and ~ 1.4 respectively and it is to be noted that, these are the locations where $\rho^{H,m}(E)$ has local peaks. For Sm, like $\rho^{H,m}(E)$, it is unimodal. At the centroid of the envelopes, the value of $\xi_2(E)$ are ~ 0.39 , ~ 0.42 and ~ 0.5 for Nd, Pm and Sm respectively. These should be compared with the EGOE(1+2) values given by Eq. (25) (for the Nd, Pm and Sm atoms, ζ^2 is 0.88, 0.86 and 0.83 respectively) and they are 0.44, 0.48 and 0.55 respectively. Here it is assumed that α value at the $\hat{\epsilon}_k = 0$ can be used for all $\hat{\epsilon}_k$'s. However this is not a good approximation as seen from Fig.6. In a better calculation we use Eq. (24), where the integral is divided into seven segments each with $\hat{\epsilon}_k$ spread .5 in the range -1.75 to 1.75. Within each segment $F_k(E)$ is constructed with α taken for the mid $\hat{\epsilon}_k$ but incorporating exact $F_k(E)$ centroids and widths. This calculation gives overall good description for Sm while for Pm there are deviations for $\hat{\epsilon}_k > 0$. This is not surprising because there is a secondary peak for $\hat{E} > 0$, which cannot be accounted in the EGOE(1+2) model adopted. For Nd we have not shown the result as the α for $\hat{\epsilon}_k = -1.0$ is undetermined. Assuming an interpolating value of α , it is seen that the calculations describe reasonably well $\xi_2(E)$ for $\hat{E} < 0$.

In Fig. 6d-f $\xi_2(E)$ is binned to remove local fluctuations and the resulting histograms are shown. They give at the center the $\xi_2(E)$ to be 0.27, 0.33 and 0.48 for Nd, Pm and Sm respectively. Finally, though the number of localized states appear numerous in the plots, they are in fact not that many. This is seen clearly from Fig. 6g-i where the relative density of localized states is plotted as a histogram. We classify a state as localized if it has $\xi_2(E)$ less than or equal to 20% of the binned value in corresponding energy range. As shown in Fig. 6g-i the number of localized states in each energy bin $\rho_{loc}(E)$ is small for all the atoms studied. This indicates the difference between the envelope and binned $\xi_2(E)$ is due to high frequency fluctuations and not due to purely localized states. In order to understand more about localized states an analysis is carried out in terms of occupancies of single electron orbits and we will turn to this now.

D. Occupation number $\langle n_\alpha \rangle^E$ and the localized states

In the statistical description of a many-body quantum system, properties of the system are often expressed as functions of the sub-shell occupation numbers [8]. In this section, we use sub-shell occupation numbers to study the nature of the localized states. By definition the occupation number of the sub-shell α in $|k\rangle$ is

$$\langle n_\alpha \rangle_k = \langle k | a_\alpha^\dagger a_\alpha | k \rangle \quad (30)$$

where a_α^\dagger and a_α are the particle creation and annihilation operators in the sub-shell α and these are defined in Section II A. Further, we can also define the sub-shell occupancy of an atomic state

$$\langle n_\alpha \rangle^E = \langle E | a_\alpha^\dagger a_\alpha | E \rangle = \sum_k |C_k^E|^2 \langle n_\alpha \rangle_k. \quad (31)$$

It is evident from $\xi_2(E)$ calculations that, there are several localized states as shown in Fig. 6g-i. Each of these have $\xi_{loc}(E) \ll \overline{\xi_2(E)}$ and few $|k\rangle$ can represent these states. A possible origin of localized states is strong Coulomb mixing

between few $|k\rangle$ of similar sub-shell occupancies, then the two-electron Coulomb integral is between same orbitals and is large ($K = 0$ multipole is allowed). This is indeed the case and the signature is the anticorrelation in the trend of $\xi_2(E)$ and occupation number of selected sub-shells shown in Fig. 7. The figures show $\xi_2(E)$ and $\langle n_\alpha \rangle^E$ of few $|E\rangle$ around centroid energy. In Fig. 7a, there is anticorrelation between the $\xi_2(E)$ and $\langle n_{5d_{3/2}} \rangle^E + \langle n_{5d_{5/2}} \rangle^E$ of Nd, similar trend is observed for Pm in Fig. 7b *i.e.* the occupancies are large when NPC is small. This shows the localized states of Nd and Pm within the spectral range considered arise from strong mixing between $|k\rangle$ of high $5d$ occupancy. Whereas, the localized states of Sm as shown in Fig. 7c arise from the strong mixing between $|k\rangle$ of high $6s$ or $6p$ occupancies.

To compare and contrast the chaotic and localized states, $|C_k^E|^2$ of pair of neighboring chaotic and localized states of Nd, Pm and Sm are shown in Fig. 8. The figures clearly shows that the localized states (energy states, $\Gamma = 800$, $\Gamma = 2148$ and $\Gamma = 2885$ of Nd, Pm and Sm respectively) are represented by few $|k\rangle$, whereas the neighboring chaotic states ($\Gamma = 801$, $\Gamma = 2149$ and $\Gamma = 2886$ of Nd, Pm and Sm respectively) has contributions from several $|k\rangle$. The $|C_k^E|^2$ of the chaotic states exhibit a systematic growth and decay, in contrast localized states show no systematic trends. To show the anticorrelation between $\langle n_\alpha \rangle$ of selected sub-shells and $\xi_2(E)$, the contributions from each basis $|C_k^E|^2 \langle n_\alpha \rangle_k$ are plotted. For the localized states the plots are for α that has the highest value. For the chaotic states, all the sub-shells show similar trend and approximately an order of magnitude less (see the scales in Fig. 8) than that of the localized states.

V. HAMILTONIAN MATRIX STRUCTURE

Understanding the structure of the Hamiltonian matrix is crucial for developing an appropriate random matrix model for the Lanthanide atoms. The diagonal Hamiltonian matrix elements H_{kk}^{DC} will have contributions from both the one and two particle Hamiltonian terms. However, the off diagonal terms $H_{kk'}^{\text{DC}}$ have non-zero contributions from the Hamiltonian terms depending on the relative excitation between $|k\rangle$ and $|k'\rangle$. If the two CSFs are singly excited with respect to each other, then one and two particle terms contributes, whereas only the two particle term contributes when the two CSFs are doubly excited with respect to each other. The off diagonal matrix elements are zero for triple or higher excitations. As a consequence, the Hamiltonian matrix is sparse. In our present calculations, several of the CSFs which are doubly excited with respect to ground configuration are quadruply excited with respect to each other. For example the configurations $4f^{m-2}5d^{n+2}6s^2$ and $4f^m5d^n6p^2$ are doubly excited with respect to the ground configuration $4f^m5d^n6s^2$, however they are quadruply excited with respect to each other. Hence, all the matrix elements between CSFs arising from $4f^{m-2}5d^{n+2}6s^2$ and $4f^m5d^n6p^2$ are zero. There are other configurations similar to these in the CI space considered. Due to these configurations, the Hamiltonian matrix in our calculations is sparse, though we consider only the single and double excitations from the ground state configuration. For bringing out a coarse grained structure of the Hamiltonian matrix, the square of matrix elements ($H_{kk'}^{\text{DC}})^2$ (to remove the phase factor) is calculated and binned in terms of the diagonal elements H_{kk}^{DC} . The element W_{ij} of the binned Hamiltonian for bin size Δ is then

$$W_{ij} = \sum_{(i'-H_{kk}) \leq \Delta, (j'-H_{ll}) \leq \Delta} H_{kl}^2 \quad (32)$$

where $i' = i \times \Delta$ and $j' = j \times \Delta$. The plot of binned Hamiltonian for Nd, Pm and Sm are shown in Fig.9. To improve the contrast the plots show $\ln(W_{ij})$ instead of the W_{ij} . In all the three atoms: (i) band like structure is evident, however, there are also block structures within the band; (ii) another important feature is the prominent streaks of large matrix elements parallel to the diagonal, these mix two diagonal blocks and, as mentioned in [39], perturbative calculation can account for these distant elements; (iii) the Hamiltonian matrices of Nd and Pm have small range of energy with no states and these are the empty stripes in the figures.

Presence of prominent diagonal blocks in the figures (point (i) above) is a consequence of the spread of the various configurations shown in Fig. 4 and Table 1. Though it is tempting to conclude that there is a BRM like structure, it should be noted that the various blocks retain their identity each with their own internal variance $\sigma^2(\tilde{m} \rightarrow \tilde{m})$. Fig. 9 clearly shows that the partial variances $\sigma^2(\tilde{m} \rightarrow \tilde{m}')$ (except in some special cases) are in general much smaller compared to the internal variances. It should be pointed out that block matrix structure as in Fig. 9 is also observed very recently in nuclear shell model calculations [40, 41] and it is plausible that such structure is a feature of interacting particle systems. In [40, 41] it is argued that one of sources for this structure is J symmetry. The various blocks are much more well separated in Nd and Pm as compared to Sm and as a result Sm is much closer to EGOE(1+2) with Nd and Pm exhibiting larger localization with departures from EGOE(1+2) predictions.

To gain better understanding of the off-diagonal matrix (i.e. (i) and (ii) above), which will mix the CSF's, let us consider their structure in some detail. In the present calculations the off diagonal Hamiltonian matrix elements $H_{kk'}^{\text{DC}}$

are largely generated by the inter-electron Coulomb interaction $1/r_{12}$ than the one electron terms t_i where,

$$t_i = c\boldsymbol{\alpha}_i \cdot \mathbf{p}_i + c^2(\beta_i - 1) - \frac{Z(\mathbf{r}_i)}{r_i} \quad (33)$$

In second quantized notation, H^{DC} can be written as

$$H^{\text{DC}} = \sum_{\alpha\beta} \langle \alpha | t | \beta \rangle a_\beta^\dagger a_\alpha + \sum_{\alpha\beta\gamma\delta} \langle \gamma\delta | \frac{1}{r_{12}} | \alpha\beta \rangle a_\gamma^\dagger a_\delta^\dagger a_\beta a_\alpha \quad (34)$$

where for short we use Greek alphabets to denote orbitals and summation is without restrictions. The two-particle matrix element of $1/r_{12}$ can be decomposed into multipole components,

$$\langle \gamma\delta | \frac{1}{r_{12}} | \alpha\beta \rangle = \sum_K G^K(\gamma, \delta; \alpha, \beta) R^K(\gamma, \delta; \alpha, \beta) \quad (35)$$

where $G^K(\gamma, \delta; \alpha, \beta)$ and $R^K(\gamma, \delta; \alpha, \beta)$ are angular and radial integrals respectively, and K is the multipole. The angular momentum selection rules are consequence of $G^K(\gamma, \delta; \alpha, \beta)$ and the radial integral also known as Slater integral [42]. In total there are $N_v^2(N_c + N_v - 1)^2/4$ matrix elements of $1/r_{12}$ which contribute to the off-diagonal Hamiltonian matrix elements; N_v and N_c are defined in Section II. The many-particle matrix elements of $1/r_{12}$ can be written as,

$$\langle \gamma_r P J M | \frac{1}{r_{12}} | \gamma_s P J M \rangle = \sum_{\alpha\beta\gamma\delta} \sum_K C_{rs}^{K, JM}(\gamma, \delta; \alpha, \beta) R^K(\gamma, \delta; \alpha, \beta) \quad (36)$$

where $C_{rs}^{K, JM}(\gamma, \delta; \alpha, \beta)$ is the angular factor which transports the single particle matrix elements to the many-particle space. The C 's consists of two components, first the angular factor in the single electron space and second a component which propagate from the single electron to many electron space. These will have complex structure when electrons of several open-shells are coupled and the distribution of the non-zero Hamiltonian matrix exhibit intricate patterns. Interestingly, nuclear shell model calculations showed that [40, 41] the angular factors generate a part of the GOE structure of the diagonal blocks. The radial integral is large for $K = 0$ in Eq. (35) and it is an allowed multipole when $\kappa_\alpha = \kappa_\gamma$ and $\kappa_\beta = \kappa_\delta$. This can couple energetically well separated configurations strongly and explain (ii) above. Finally, from the matrix structure one can understand qualitatively the departures of $F_k(E)$ and $\xi_2(E)$ from EGOE(1+2). In this random matrix ensemble the two-particle matrix elements variance (the parameter v^2 in Eq. (18)) is independent of its position (i.e. independent of the indices (i, j, k, l) in Eq. (18) except that the diagonal matrix elements have twice the variance of the off-diagonal matrix elements).

VI. CONCLUSIONS AND FUTURE OUTLOOK

In this paper wavefunctions of complex lanthanide atoms Nd, Pm and Sm are analyzed in terms of strength functions, number of principal components, occupation numbers and also the Hamiltonian matrix structure. Examination of $F_k(E)$ showed that the BW form is dominant in Nd, they are more towards Gaussian in Pm and quite close to Gaussian in Sm for the basis states not very far from the ϵ_k centroids. All three atoms exhibit BW form for $\hat{\epsilon}_k < -1$. Thus the statistical spectroscopy developed by Flambaum et al [5-7] will be good for as long as $F_k(E)$ with $\hat{\epsilon}_k \lesssim -1$ contribute to observables of interest. In all these atoms there are localized states throughout the spectrum (though the density is not high) and this is clearly seen in the measure NPC. The structure of the localized states is closely correlated with the occupation numbers. All these and the matrix structures showed that EGOE(1+2) need to be modified. One approach is to partition the two-particle space and employ different variances for different block matrices and then propagate the ensemble to many particle spaces. Very few properties of these partitioned ensembles ($p - \text{EGOE}(1+2)$) are known till now [11] and clearly they should be studied in more detail. The induced TBRE introduced recently [43] are closely related to p-EGOE(1+2). Another approach is consider the two-particle Hamiltonian as a mixture of a regular part (say determined by the lower order multipoles in Eq.(36)) and a random part and analyze them as a function of the strength of the random part (they are called $K + \alpha \text{EGOE}(2)$ in [11] where K is a fixed operator, and numerically some studies of such an ensemble are carried out using nuclear shell model recently [12]). Thus an important outcome of the present detailed analysis (presented in Sections II-V) is that for further progress in understanding the wavefunction structure in complex atoms it is necessary to analyse various modified EGOE's and this is for future.

-
- [1] W. C. Martin, R. Zalubas, and L. Hagan, *Atomic Energy Levels – The Rare-Earth Elements*, Natl. Bur. Stand. Ref. Data Se., Natl. Bur. Stand. (U. S.), NBS-60, (U. S., GPO, Washington, DC, 1978).
- [2] V. V. Flambaum, A. A. Gribakina, G. F. Gribakin, and M. G. Kozlov, Phys. Rev. A **50**, 267 (1994).
- [3] V. V. Flambaum, A. A. Gribakina, G. F. Gribakin, and I. V. Ponomarev, Physica D **131**, 205(1999).
- [4] A. Cummings, G. O’Sullivan, and D. M. Heffernan, Journal of Phys. B **34**, 3407 (2001).
- [5] V. V. Flambaum, and F. M. Izrailev, Phys. Rev. E **56**, 5144 (1997).
- [6] V. V. Flambaum, A. A. Gribakina, G. F. Gribakin, and I. V. Ponomarev, Phys. Rev. E **57**, 4933 (1998); A. A. Gribakina, G. F. Gribakin, and V. V. Flambaum, Aust. J. Phys. **52**, 443 (1999).
- [7] V. V. Flambaum, G. F. Gribakin, and F. M. Izrailev, Phys. Rev. E **53**, 5729 (1996); V. V. Flambaum, A. A. Gribakina, and G. F. Gribakin, Phys. Rev. A **58**, 230 (1998).
- [8] V. V. Flambaum, A. A. Gribakina, G. F. Gribakin, and C. Harabati, Phys. Rev. A **66**, 012713 (2002).
- [9] G. F. Gribakin and S. Sahoo, J. Phys. B **36**, 3349 (2003).
- [10] T. A. Brody, J. Flores, J. B. French, P. A. Mello, A. Pandey, and S.S.M. Wong, Rev. Mod. Phys. **53**, 385 (1981).
- [11] V. K. B. Kota, Phys. Rep. **347**, 223 (2001).
- [12] V. Velázquez, and A. P. Zuker, Phys. Rev. Lett. **88**, 072502 (2002); V. Velázquez, J. G. Hirsch, A. Frank, and A. P. Zuker Phys. Rev. C **67**, 034311 (2003).
- [13] V. K. B. Kota, Ann. Phys. (N.Y.) **306**, 58 (2003).
- [14] Ph. Jacquod, and A. D. Stone, Phys. Rev. Lett. **84**, 3938 (2000); Y. Alhassid, Ph. Jacquod, and A. Wobst, Phys. Rev. B **61**, R13357 (2000); T. Papenbrock, L. Kaplan, and G. F. Bertsch, Phys. Rev. B **65**, 235120 (2002).
- [15] B. Georgeot, and D. L. Shepelyansky, Phys. Rev. E **62**, 3504 (2000); G. P. Berman, F. Borgonovi, F. M. Izrailev, and V. I. Tsifrinovich, *ibid.* **65**, 015204 (2001); V. V. Flambaum and F. M. Izrailev, *ibid.* **64**, 026124 (2001).
- [16] G. P. Berman, F. Borgonovi, F. M. Izrailev, and A. Smerzi Phys. Rev. Lett. **92**, 030404 (2004).
- [17] D. Angom and V. K. B. Kota, Phys. Rev. A **67**, 052508 (2003).
- [18] D. Angom, S. Ghosh and V. K. B. Kota, Phys. Rev. E **70**, 016209 (2004).
- [19] J. Bauche and C. Bauche-Arnault, Comp. Phys. Rep. **12**, 1 (1990).
- [20] D. Angom, I. Endo, A. Fukumi, M. Iinuma, T. Kondo, and T. Takahashi The Europ. Phys. Jour. D, **14**, 271 (2001); S. G. Porsev, Phys. Rev. A **56**, 3535 (1997).
- [21] C. Froese Fischer, T. Brage and P. Jönsson, *Computational Atomic Structure an MCHF Approach* (Inst. of Phys, London, 2000).
- [22] I. P. Grant, in *Methods in Computational Chemistry*, Vol. 2, edited by S. Wilson (Plenum, New York, 1988), p. 1.
- [23] F. A. Parpia, C. Froese Fischer and I. P. Grant, Comp. Phys. Comm. **94**, 249 (1996); L. Visscher, O. Visser, P. J. C. Aerts, H. Merenga, and W. C. Nieuwpoort, Comp. Phys. Commun. **81**, 120 (1994); K. G. Dyall, I. P. Grant, C. T. Johnson, F. A. Parpia, and E. P. Plummer, Comp. Phys. Comm. **55**, 425 (1989); J. P. Desclaux, D. F. Mayers, and F. O’Brien J. Phys. B **4**, 631 (1971).
- [24] B. R. Judd in *Atomic, Molecular and Optical Physics Handbook* edited by G. W. F. Drake (AIP, New York, 1996), p. 56 and p. 88; T. Kagawa, Y. Honda, and S. Kiyokawa, Phys. Rev. A **44**, 7092 (1991).
- [25] K. K. Mon, and J. B. French, Ann. Phys. (N.Y.) **95**, 90 (1975); L. Benet, T. Rupp, and H. A. Weidenmüller, Ann. Phys. (N.Y.) **292**, 67 (2001).
- [26] A. Stuart, and J. K. Ord, Kendall’s Advanced Theory of Statistics, fifth edition of Volume 1: Distribution Theory (Oxford University Press, New York, 1987).
- [27] Ph. Jacquod, and D. L. Shepelyansky, Phys. Rev. Lett. **79**, 1837 (1997).
- [28] Ph. Jacquod, and I. Varga, Phys. Rev. Lett. **89**, 134101 (2002).
- [29] I. Varga, and J. Pipek, Phys. Rev. E **68**, 026202 (2003).
- [30] V. K. B. Kota, and R. Sahu, Phys. Rev. E **64**, 016219 (2001).
- [31] M. Abramowitz, I. A. Stegun (Eds.), Handbook of Mathematical functions, NBS Applied Mathematics Series, Vol. 55, (U.S. Govt. Printing Office, Washington, D.C., 1964).
- [32] V. K. B. Kota, and R. Sahu, Phys. Rev. E **66**, 037103 (2002); M. Horoi, V. Zelevinsky, and B. A. Brown, Phys. Rev. Lett. **74**, 5194 (1995).
- [33] V. K. B. Kota, and K. Kar, Phys. Rev. E **65**, 026130 (2002).
- [34] T. Papenbrock, and H. A. Weidenmüller, Phys. Rev. Lett **93**, 132503 (2004).
- [35] J. M. G. Gómez, K. Kar, V. K. B. Kota, J. Retamosa, and R. Sahu, Phys. Rev. C **64**, 034305 (2001); M. Horoi, J. Kaiser, and V. Zelevinsky, Phys. Rev. C **67**, 054309 (2003); J. M. G. Gómez, K. Kar, V. K. B. Kota, R. A. Molina and J. Retamosa, Phys. Rev. C **69**, 057302 (2004).
- [36] V. K. B. Kota and R. Sahu, Phys. Rev. E **62**, 3568 (2000).
- [37] F. S. Chang, J. B. French, and T. H. Thio, Ann. Phys. (N.Y.) **66**, 137 (1971); S. S. M. Wong, Nuclear Statistical Spectroscopy (Oxford University Press, New York, 1986).
- [38] G. F. Gribakin, S. Sahoo and V. Dzuba ArXiv:physics/0401157.
- [39] A. A. Gribakina, V. V. Flambaum and G. F. Gribakin, Phys. Rev. E **52**, 5667 (1995).
- [40] V. Zelevinsky, B.A. Brown, N. Frazier, and M. Horoi, Phys. Rep. **276**, 85 (1996).
- [41] T. Papenbrock and H. A. Weidenmüller, arXiv:nucl-th/0403041.
- [42] I. Lindgren and J. Morrison, *Atomic Many-Body Theory* 2nd ed (Springer-Verlag, Berlin, 1986).

[43] Y. Alhassid, H. A. Weidenmueller and A. Wobst arXiv:cond-mat/0406495.

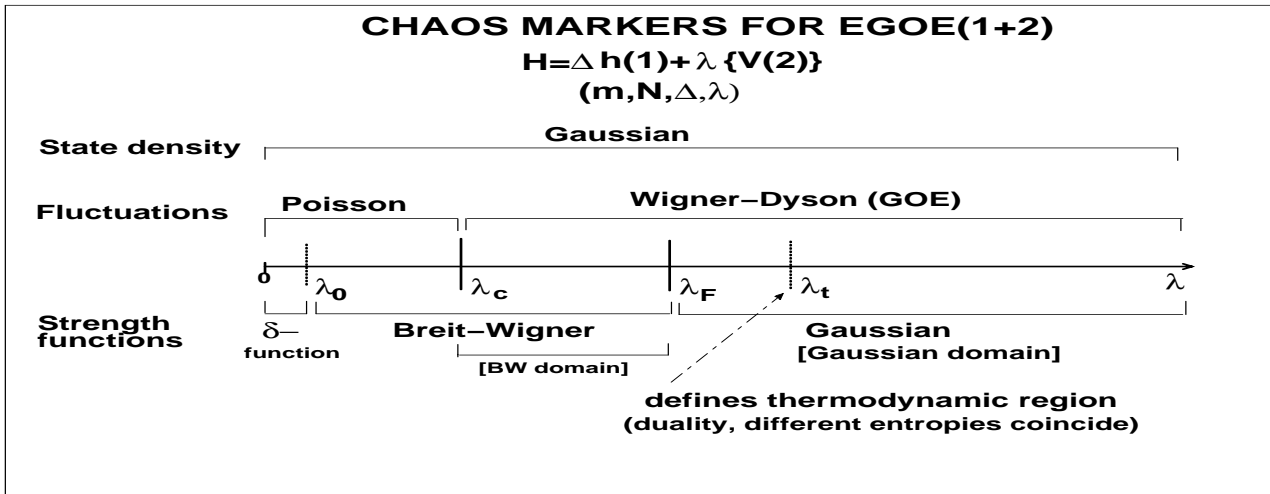
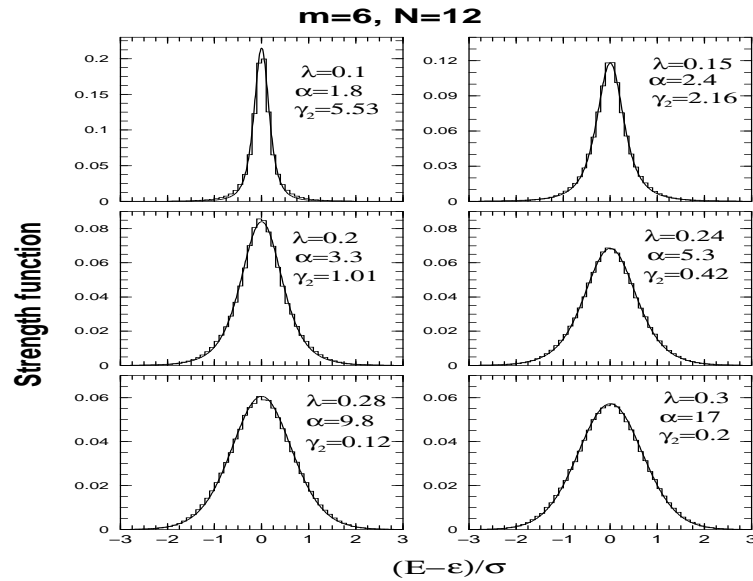


FIG. 1: Chaos markers for EGOE(1+2)

FIG. 2: Strength functions for EGOE(1+2) as a function of the interaction strength λ .

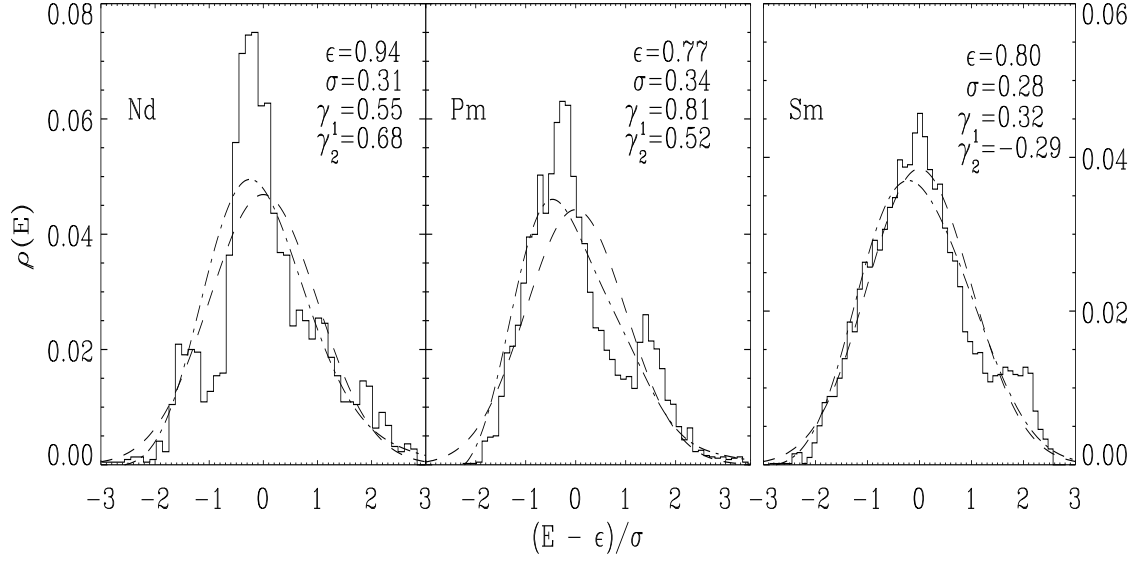


FIG. 3: Binned density of states $\rho(E)$ of Nd, Pm and Sm. The dashed and dash-dot curves are the Gaussian and Edgeworth corrected Gaussian representations.

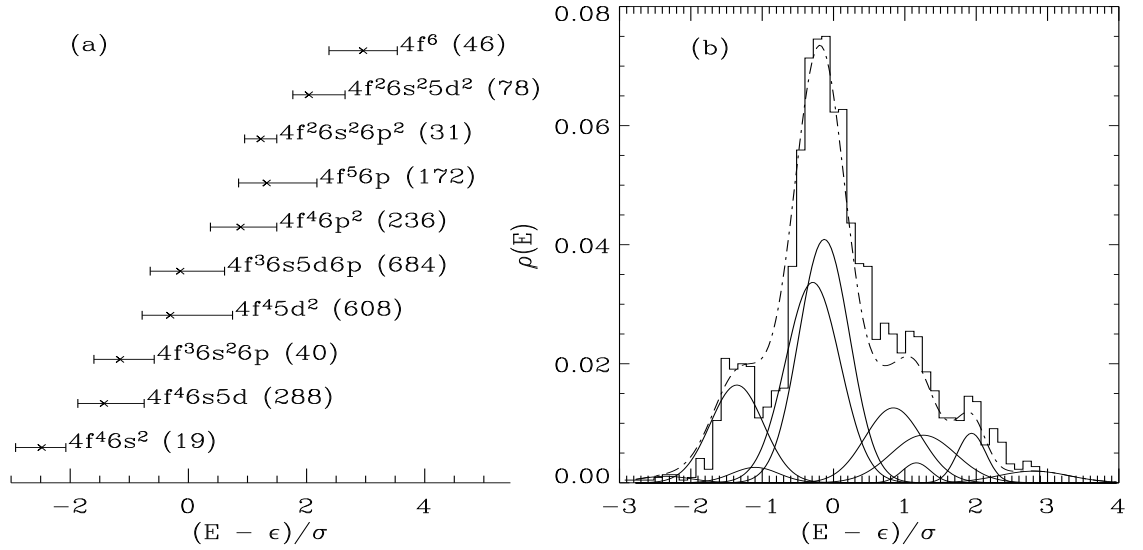


FIG. 4: (a) The energy range of CSFs for Nd arising from a non-relativistic configuration. The energies are calculated with respect to the lowest CSF energy within the manifold (-9625.2394 hartree). The number of CSFs are given within parentheses and the cross marks the location of the centroid. (b) The solid and dot-dash line are partial Gaussian densities $\rho^{H,\bar{m}}(E)$ of each non-relativistic configurations and sum of all the partial densities respectively. The histogram is that of the density of states $\rho^H(E)$.

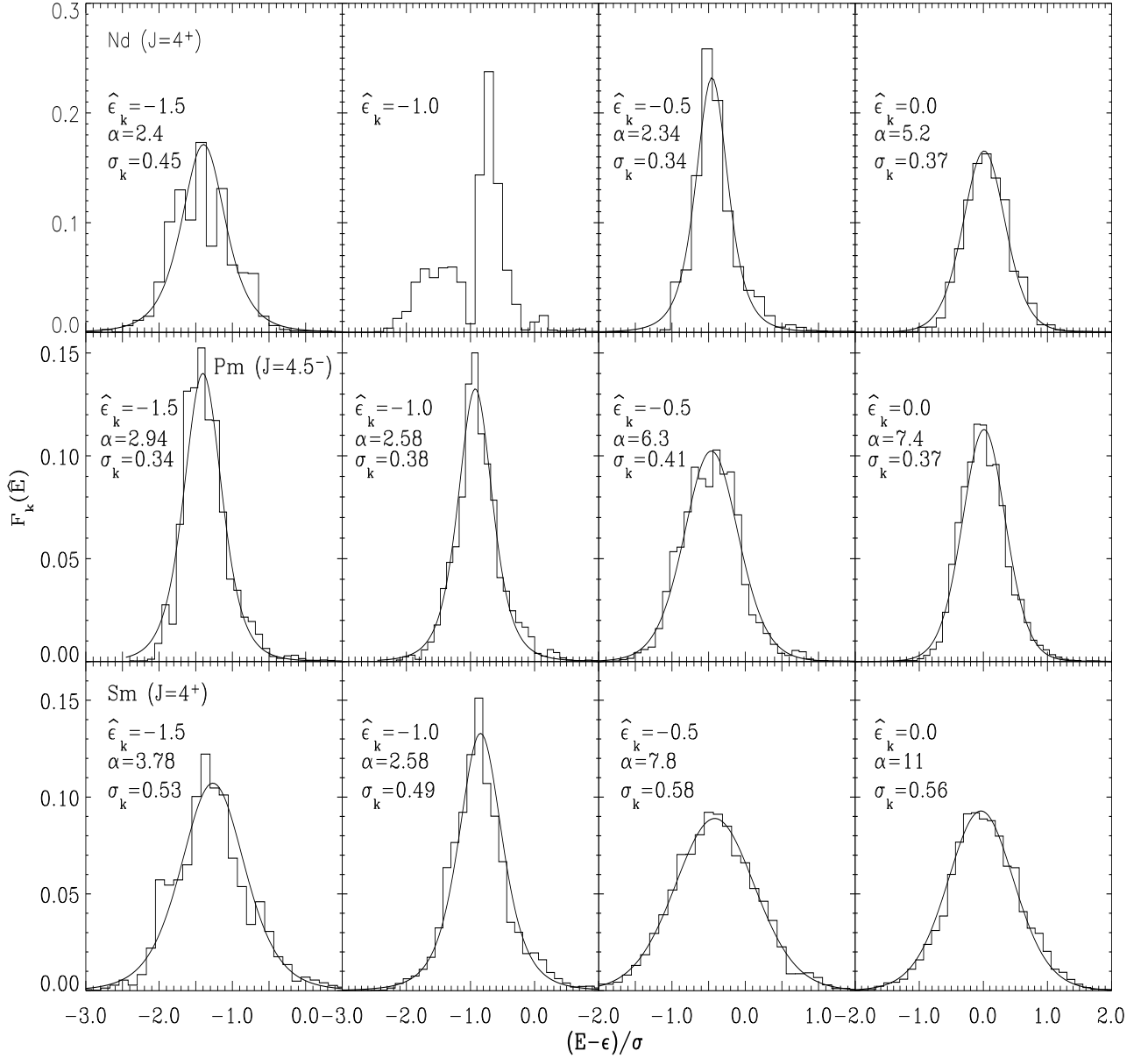


FIG. 5: The plots in the three rows are the averaged strength function $\overline{F_k(\hat{E})}$ for Nd, Pm and Sm respectively. As labeled in the plots, the plots in the four columns show $F_k(\hat{E})$ averaged in the range $-1.5 \pm 0.25\sigma_k$, $-1.0 \pm 0.25\sigma_k$, $-0.5 \pm 0.25\sigma_k$, and $0.0 \pm 0.25\sigma_k$ respectively.

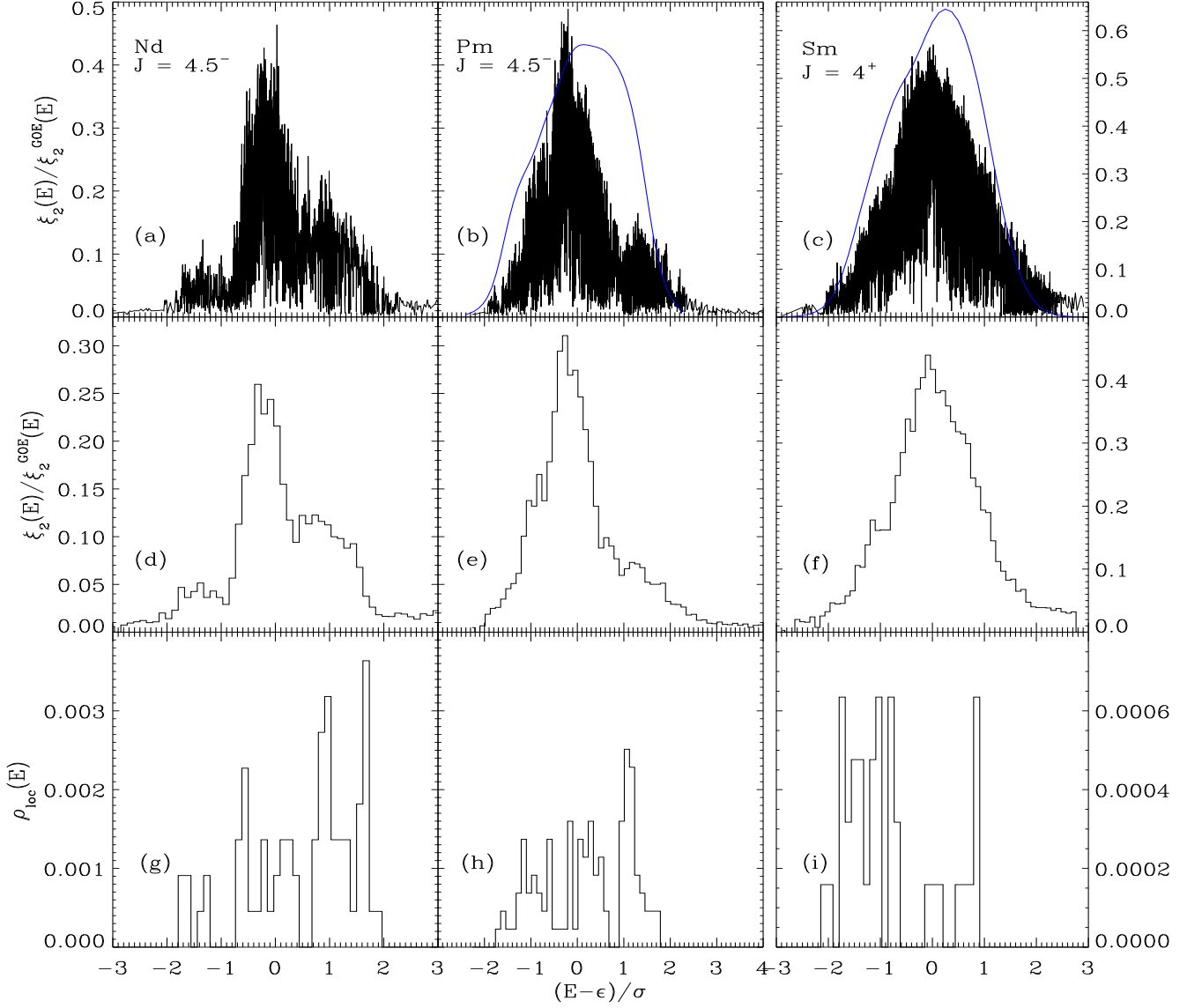


FIG. 6: The number of principal components $\xi_2(E) = (\sum_k |C_k^E|^4)^{-1}$ of Nd I, Pm I and Sm I are plotted in the first row. The plots in the second row are binned $\xi_2(E)$ and the last row is the binned density of localized states $\rho_{\text{loc}}(E)$. In (b) and (c) the continuous curves are from Eq. (24) as described in the text.

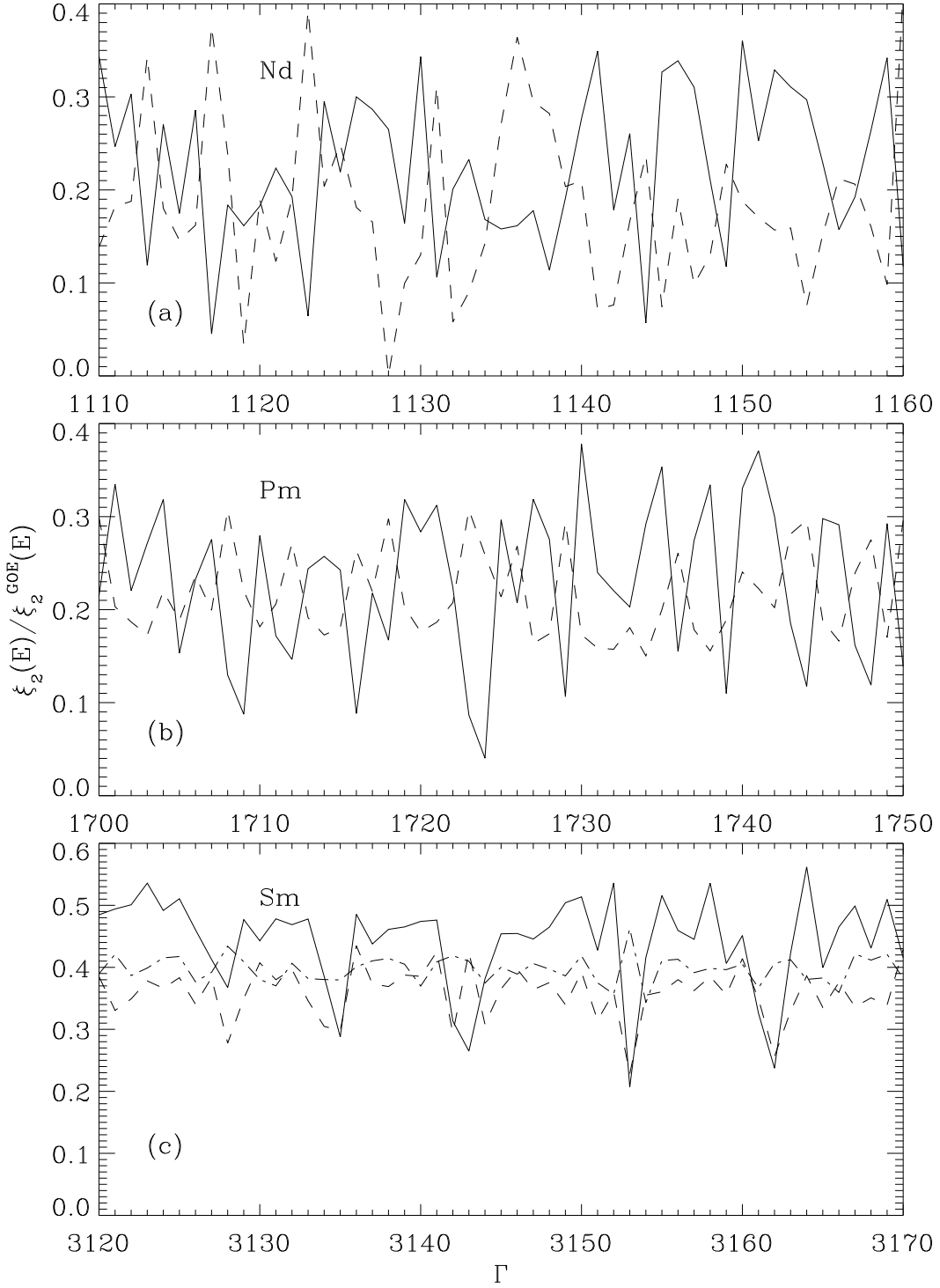


FIG. 7: The solid line is the number of principal components $\xi_2(E)$ of energy states Γ around the centroid. The dot-dash line show the occupation number $\langle n_\alpha \rangle^E$ of selected shells which anti-correlate with the localized states. The occupation numbers are scaled and shifted for better comparison with $\xi_2(E)$: for Nd the plot shows $\langle n_{5d_{3/2}} \rangle^E + \langle n_{5d_{5/2}} \rangle^E - 1$, for Pm it is $0.2(\langle n_{5d_{3/2}} \rangle^E + \langle n_{5d_{5/2}} \rangle^E)$ and for Sm the dot-dash and dashed lines are $\langle n_{6s_{1/2}} \rangle^E - 3$ and $\langle n_{6p_{1/2}} \rangle^E + \langle n_{6p_{3/2}} \rangle^E - 3$ respectively.

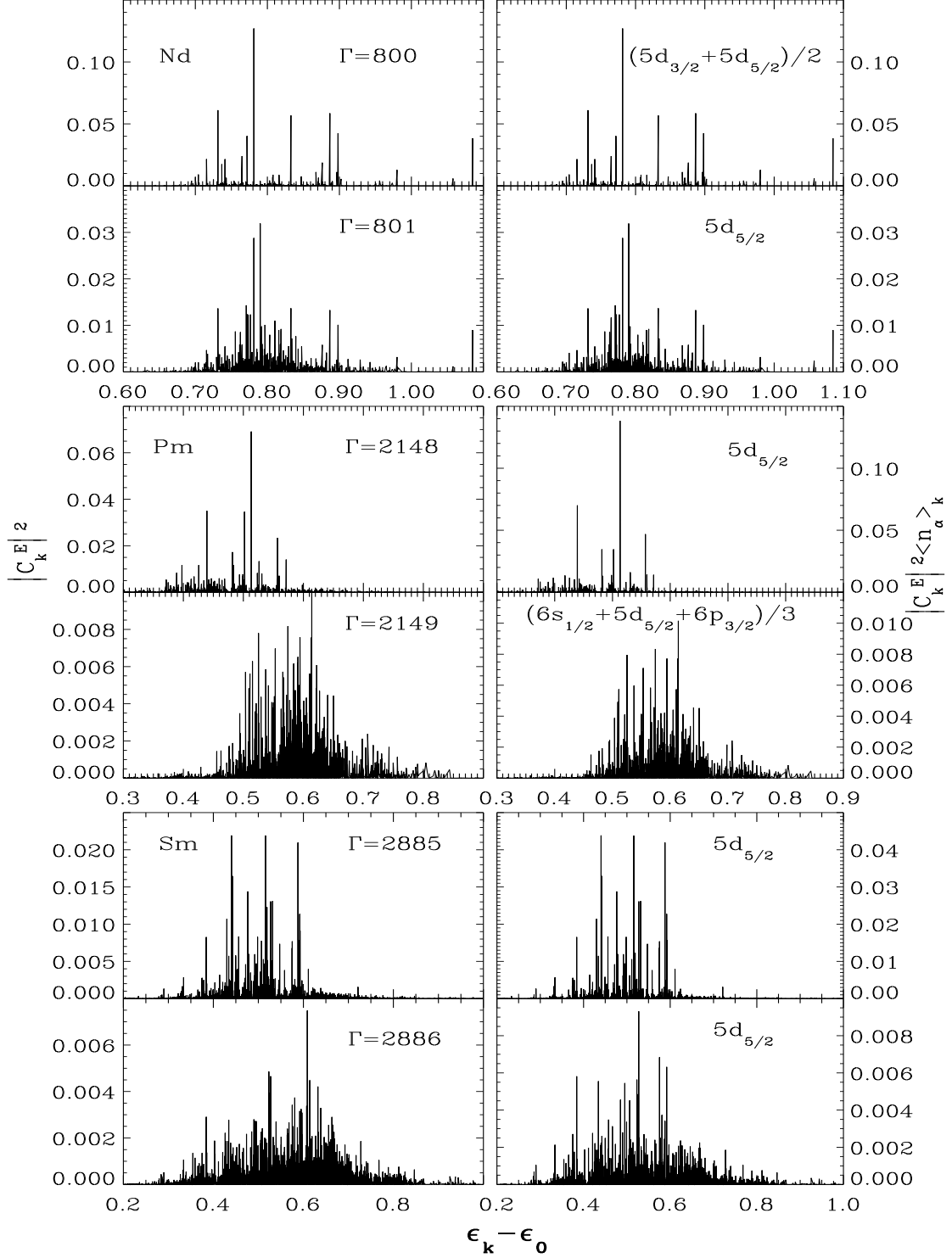


FIG. 8: The $|C_k^E|^2$ of neighboring localized and chaotic pair of $|E\rangle$ are shown in the plots in the first column. Even though each pair are neighboring states, a large difference in the structure is discernable. For the localized states, the second column shows the individual $|k\rangle$ contribution $|C_k^E|^2 \langle n_\alpha \rangle_k$ to the sub-shell of highest $\langle n_\alpha \rangle$, whereas for chaotic states all the sub-shells have similar $|C_k^E|^2 \langle n_\alpha \rangle_k$ and the plots show contribution from a randomly chosen sub-shell.

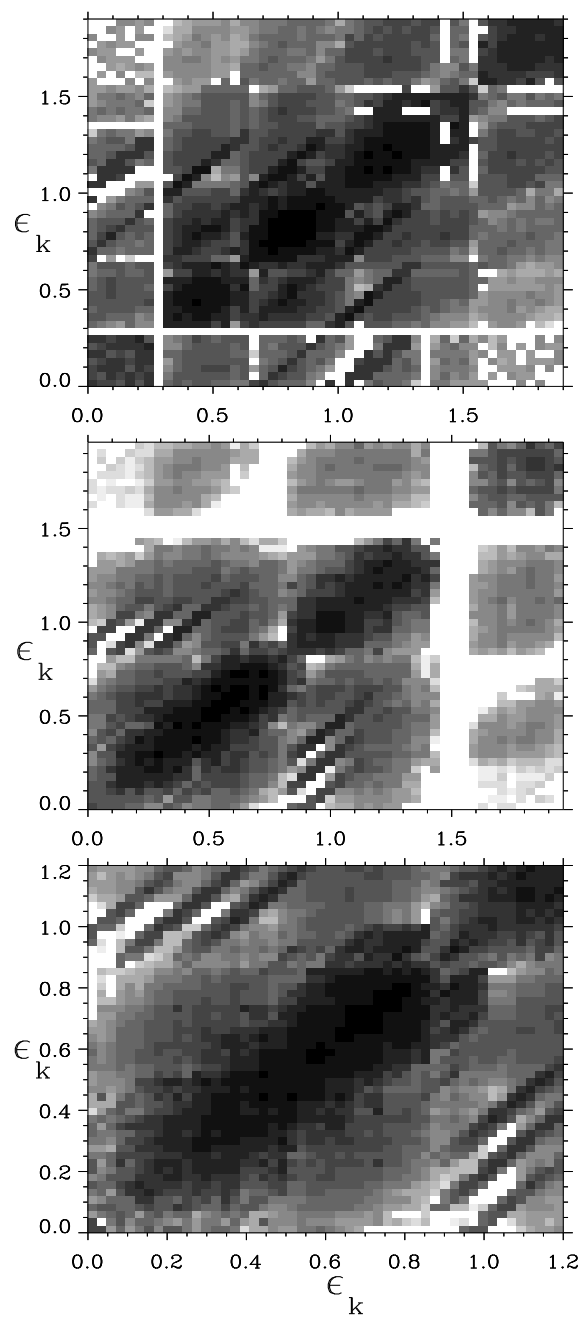


FIG. 9: The binned Hamiltonian matrix of Nd I, Pm I and Sm I.